

Coupling curvature-dependent and shear stress-stimulated neotissue growth in dynamic bioreactor cultures: a 3D computational model of a complete scaffold

Y. Guyot^{1,2} · I. Papantoniou^{1,3} · F. P. Luyten^{1,3} · L. Geris^{1,2,4}

Received: 13 February 2015 / Accepted: 13 December 2015 / Published online: 12 January 2016
© Springer-Verlag Berlin Heidelberg 2016

Abstract The main challenge in tissue engineering consists in understanding and controlling the growth process of in vitro cultured neotissues toward obtaining functional tissues. Computational models can provide crucial information on appropriate bioreactor and scaffold design but also on the bioprocess environment and culture conditions. In this study, the development of a 3D model using the level set method to capture the growth of a microporous neotissue domain in a dynamic culture environment (perfusion bioreactor) was pursued. In our model, neotissue growth velocity was influenced by scaffold geometry as well as by flow-induced shear stresses. The neotissue was modeled as a homogenous porous medium with a given permeability, and the Brinkman equation was used to calculate the flow profile in both neotissue and void space. Neotissue growth was modeled until the scaffold void volume was filled, thus capturing already established experimental observations, in particular the differences between scaffold filling under different flow regimes. This tool is envisaged as a scaffold shape and bioprocess optimization tool with predictive capacities. It will allow controlling fluid flow during long-term culture,

whereby neotissue growth alters flow patterns, in order to provide shear stress profiles and magnitudes across the whole scaffold volume influencing, in turn, the neotissue growth.

Keywords 3D neotissue growth · Shear stress influence · Fluid flow · Bioreactor · Numerical modeling

1 Introduction

Skeletal tissue engineering (TE) strategies hold a great promise for the regeneration of bone and cartilage based on the combination of bioreactors, 3D biomaterials and mesenchymal stem cells (MSCs). MSCs are progenitor cells crucial for skeletal TE applications due to their ability to undergo osteogenic and chondrogenic differentiation under the influence of various biochemical, biophysical and, importantly, biomechanical cues. Perfusion bioreactors have been extensively employed for the expansion and differentiation of MSCs providing sufficient mass transport for cell growth and differentiation (Sikavitsas et al. 2005; Grayson et al. 2011; Sonnaert et al. 2014). Furthermore, shear stress can determine early stem cell lineage commitment (Song et al. 2013) but also promote terminal osteogenic differentiation of bone marrow, periosteum and adipose-derived MSCs and enhance extracellular matrix (ECM) deposition (McCoy et al. 2010; Rauh et al. 2011; Papantoniou et al. 2013). There is a substantial body of the literature illustrating the osteogenic effect of mechanical stimulation either due to fluid flow or mechanical compression (or stretching) on the differentiation of MSCs when cultured in dynamic environments seeded on 3D scaffolds in vitro (Wang et al. 2013; Delaine-Smith et al. 2011).

In scaffold-based perfusion bioreactor culture, 3D cell growth and neotissue formation have been observed to begin with 2D cell proliferation on the scaffold strut surface. Subse-

✉ Y. Guyot
yguyot@ulg.ac.be

¹ Prometheus, Division of Skeletal Tissue Engineering, KU Leuven, Onderwijs en Navorsing 1 (+8), Herestraat 49, PB 813, 3000 Leuven, Belgium

² Biomechanics Research Unit, Universite de Liege, Chemin des Chevreuils 1 - BAT 52/3, 4000 Liège, Belgium

³ Skeletal Biology and Engineering Research Center, KU Leuven, Onderwijs en Navorsing 1 (+8), Herestraat 49, PB 813, 3000 Leuven, Belgium

⁴ Department of Mechanical Engineering, Biomechanics Section, KU Leuven, Celestijnenlaan 300C, PB 2419, 3001 Leuven, Belgium

quently, cells bridge scaffold struts and start growing toward the pore void followed by ECM deposition. Eventually, 3D cell growth will result in scaffold void filling, something that has been studied recently using computed tomography imaging techniques (Voronov et al. 2013; Papantoniou et al. 2014). The calculation of wall shear stress values in empty scaffold geometries are therefore indicative of the shear stress experienced by cells during early culture time (Truscello et al. 2011). A current challenge to further advance and utilize computational modeling strategies in the TE field is to comprise a domain composed of cells and ECM (a growing permeable neotissue) on real 3D scaffold geometries. There are intriguing 2D studies investigating this (Sacco et al. 2011; Hossain et al. 2014); however, it was recently shown that without the third dimension, model parameters were overestimated, losing accuracy in the representation of neotissue growth (Nava et al. 2013).

Computational fluid dynamics (CFD) modeling has been extensively used in the field of TE [for review, see Hutmacher et al. (2008), Hossain et al. (2012), Patrachari et al. (2012)]. The quantification of flow-associated shear stresses as well as their spatial distribution within various 3D scaffold geometries has been thoroughly investigated in perfused bioreactor setups (Raimondi et al. 2004; Porter et al. 2005; Boschetti et al. 2006; Cioffi et al. 2006; Jungreuthmayer et al. 2009; Maes et al. 2009; Voronov et al. 2010). In previous studies, local shear stresses were defined as a function of flow rate of the culture medium, bioreactor configuration, porosity and porous scaffold microarchitecture (Voronov et al. 2010; Pham et al. 2012). Most 3D CFD studies to date only use empty scaffold geometries to calculate shear stress magnitude and distribution across the empty scaffold surface, i.e., wall shear stress. The aforementioned studies do not take into account the transient nature of the 3D neotissue domain as a result of neotissue growth which has been observed experimentally (Papantoniou, Sonnaert et al. 2014). There have been few attempts to capture 3D neotissue growth on scaffolds, limited to gradually increasing scaffold struts (Lesman et al. 2010), representing the neotissue layer as an impermeable domain. A recent interesting study describes the growth of a ‘biomass’ domain (similar to what we term neotissue in this study) whose growth was coupled to oxygen concentration and shear stress (Nava et al. 2013).

In addition to flow-associated shear stress, neotissue growth kinetics have been also linked to the geometric features of scaffolds. Pore size (Zeltinger et al. 2001), pore shape (Knychala et al. 2013) and more specific features such as local curvature (Rumpler et al. 2008; Gamsjager et al. 2013) have been demonstrated to control cell fate for both in vitro (Rumpler et al. 2008; Guyot et al. 2014) and in vivo applications (Bidan et al. 2012).

Building on our previous studies where we investigated the effect of local curvature on in vitro 3D growth (Guyot et al.

2014) and where we used the evolving neotissue growth in a 3D scaffold to accurately determine the shear stress values in both the void space and the neotissue during the bioreactor culture process (Guyot et al. 2015), this study demonstrates the added value of using also the shear stress as a parameter that influences the neotissue growth. Hereto this study shows the development of a level-set-based computational tool able to capture the difference in growth of a microporous neotissue domain in a dynamic culture environment (perfusion bioreactor) under different flow rates. Capturing this difference is only possible by the explicit incorporation of flow-induced shear stresses as a parameter in the calculation of the neotissue growth velocity [alongside the scaffold geometry which was already present (Guyot et al. 2014)]. This tool provides the ability to steer fluid flow during long-term culture in order to provide given shear stress profiles and magnitudes across the whole scaffold volume.

2 Methods

In this section, the model describing the neotissue growth, the calculation of the flow-induced shear stresses and the influence of the latter on the former will be explained.

2.1 Neotissue growth via the level set method

The growth-induced changes in the neotissue topology during the culture process can be seen as a moving interface between two different domains (Sethian 1999): In this study, one domain represents the neotissue volume Ω_{nt} , and the other one is the void Ω_v , separated by an interface Γ , with a normal \mathbf{n}_Γ (see Fig. 1b). The level set method (LSM) is a technique that has been developed to deal with this kind of moving interfaces, and it is used in the context of this study to simulate the evolution of the frontline Γ between neotissue and void space in a mesh-free manner. The principle of the LSM consists in defining a signed distance function φ in $\Omega = \Omega_{nt} \cup \Omega_v$ with the following properties:

$$\begin{cases} \varphi > 0 & \text{in } \Omega_{nt} \\ \varphi < 0 & \text{in } \Omega_v \\ \varphi = 0 & \text{on } \Gamma \end{cases} \quad (1)$$

In order to capture the evolution of the moving interface Γ , the following transient advection equation is solved with a given growth velocity \mathbf{v}_G and homogenous Neumann boundary condition ($\partial\varphi/\partial\mathbf{n} = 0$, with \mathbf{n} being the normal to the computational domain Ω).

$$\frac{\partial\varphi}{\partial t} + \mathbf{v}_G \cdot \nabla\varphi = 0 \text{ in } \Omega. \quad (2)$$

With $\mathbf{v}_G = V_G * \mathbf{n}_\Gamma$, and $\mathbf{n}_\Gamma = \frac{\nabla\varphi}{|\nabla\varphi|}$. The expression of the growth velocity magnitude V_G will be described later. The

initial configuration of the distance function φ corresponds to a homogenous single cell layer over the scaffold struts with a thickness equal to $20\ \mu\text{m}$ (Darling et al. 2008). The time discretization of Eq. (2) was done using the backward Euler method, and the advection term was treated with the method of characteristics. For more details about the implementation, please refer to (Guyot et al. 2014).

2.2 Shear stress distribution

During dynamic culture, the neotissue grows, eventually filling up the whole scaffold void. These changes affect the flow patterns developed, depending on the presence (or not) of neotissue, and so the flow profile has to be treated differently in Ω_{nt} and Ω_{v} [as described in detail in Guyot et al. (2015)]. In Ω_{v} , due to a low Reynolds number ($Re < 1$), the flow profile was approximated via the Stokes Eq. (3). In Ω_{nt} , the complex structure of the neotissue can be seen as a homogenous porous medium with a given permeability K_0 , leading to the flow profile being calculated with the Darcy Eq. (4). According to the definition of the LSM, the interface Γ is never conforming to the computational mesh, resulting in difficulties to couple Eqs. (3) and (4) together with suitable boundary conditions at the interface. To overcome this, the Brinkman Eq. (5) was used to calculate the flow profile in the whole domain Ω (see Fig. 1c). A no-slip boundary condition was applied on the scaffold surface as well as on the chamber walls. The scaffold was placed at a sufficient distance from the inlet avoiding refluxes occurring at the entrance of the scaffold (Papantoniou et al. 2014), so the boundary condition for the inflow was set to a Poiseuille profile with a velocity u corresponding to the given flow rate Q .

$$\begin{cases} -\mu \Delta \mathbf{u} + \nabla p = 0 & \text{in } \Omega_{\text{v}} \\ \nabla \cdot \mathbf{u} = 0 & \text{in } \Omega_{\text{v}} \end{cases} \quad (3)$$

$$\begin{cases} \frac{\mu}{K_0} \mathbf{u} + \nabla p = 0 & \text{in } \Omega_{\text{nt}} \\ \nabla \cdot \mathbf{u} = 0 & \text{in } \Omega_{\text{nt}} \end{cases} \quad (4)$$

$$\begin{cases} -\mu \Delta \mathbf{u} + \nabla p + \frac{\mu}{K} \mathbf{u} = 0 & \text{in } \Omega \\ \nabla \cdot \mathbf{u} = 0 & \text{in } \Omega \end{cases} \quad (5)$$

This technique can be seen as a penalization method; indeed, when K is equal to the neotissue permeability ($K \ll 1$) in Ω_{nt} , it makes the Stokes term in (5) negligible. At the contrary, when K is set to a very high value ($K \gg 1$) in Ω_{v} , it leads to the Darcy term to be close to zero. To avoid numerical problems, this switch between the two values was implemented using a space- and time-dependent smeared-out Heaviside function H (6), and K was updated according to this function (7) ($\varepsilon = 1.5$ h, with h the mesh size).

$$H(\varphi) = \begin{cases} 0, & \varphi < -\varepsilon \\ \frac{1}{2} + \frac{\varphi}{2\varepsilon} + \frac{1}{2\pi} \sin\left(\frac{\pi\varphi}{\varepsilon}\right), & -\varepsilon < \varphi < \varepsilon \\ 1, & \varphi > \varepsilon \end{cases} \quad (6)$$

$$K(\mathbf{x}) = 10^{30}(1 - H) + K_0 H \quad (7)$$

The parameter K_0 was estimated using the random fibers theory approximation. In Nabovati et al. (2009), the authors provide an approximation of the permeability of a porous media made of a random fiber web:

$$K_0 = 0.491\delta^2 \sqrt{\frac{1 - \psi_c}{1 - \psi}}^{-2.31}. \quad (8)$$

In this equation, ψ represents the porosity of the media (neotissue, assumed to be equal to 90 % in this study, which is in the range of porosities of soft tissues and hydrogels) and ψ_c corresponds to a percolation threshold or a threshold porosity where flow is permitted (set to zero in this study). Finally, δ represents the micropore size of the neotissue and was set to $50\ \mu\text{m}$, assuming the pore size equal to half to one-third of the size of a fully spread cell of the type used in this study (Eyckmans et al. 2012).

In this study, we distinguished two different wall shear stresses acting on cells depending on their location. The first one (SS_{surf}) is the shear stress acting on the interface Γ due to the different flow profiles from either side and is calculated with the usual definition:

$$SS_{\text{surf}} = \sqrt{\tau_{12}^2 + \tau_{23}^2 + \tau_{13}^2}, \quad \text{with} \quad \tau_{ij} = \mu \left(\frac{\partial u_i}{\partial x_j} + \frac{\partial u_j}{\partial x_i} \right). \quad (9)$$

The second one (SS_{in}) is the shear stress acting within the neotissue, and it is associated with the interstitial flow through the microporous neotissue and is approximated following the method presented in Whittaker et al. (2009). This method is based on the fact that the microporous neotissue is assumed to be composed of cylindrical ducts of diameter δ . Since the Darcy equation just gives the average (Darcy) velocity u , the interstitial velocity magnitude u_{in} is calculated from results of Eq. (5) and is turned into a Poiseuille velocity profile (u_{p}) in a cylindrical channel in order to have an analytical expression of local wall shear stress (on the wall of the cylindrical ducts, representing here the micropores), allowing for the estimation of SS_{in} .

$$u_{\text{in}} = |\mathbf{u}| / \psi \quad (10)$$

$$u_{\text{p}} \approx 2u_{\text{in}} \left(1 - \left(\frac{2r}{\delta} \right)^2 \right) \quad (11)$$

$$SS_{\text{in}} = \mu \left| \frac{\partial u_{\text{p}}}{\partial r} \right|_{r=\delta/2} \approx \frac{8\mu u_{\text{in}}}{\delta} \approx \frac{8\mu |\mathbf{u}|}{\delta\psi} \quad (12)$$

2.3 Neotissue growth velocity

A key parameter of the study is the local growth velocity of the neotissue. In [Guyot et al. \(2014\)](#), this space-dependent velocity was only depending on the local mean curvature of the interface as it has been shown in [Bidan et al. \(2012\)](#) or [Rumpler et al. \(2008\)](#). Another important growth-influencing factor is the local shear stress on cells. In [Nava et al. \(2013\)](#), authors present a biomass growth model for cartilage describing an interface moving in time in function of the fluid-induced shear stress, and in [Chapman et al. \(2014\)](#), the authors introduce a growth model for cell aggregates in hollow fiber bioreactors where cell population growth increased or decreased depending on wall shear stresses experienced by cells. In this study, a similar approach is used and the local neotissue growth velocity V_G is described as a function of both the mean curvature and the flow-induced shear stress:

$$V_G = A \cdot f(SS_{\text{surf}}) \cdot g(\kappa). \quad (13)$$

The neotissue growth velocity parameter A was estimated from the experimental data obtained for the low-flow-rate results obtained in [Papantoniou et al. \(2014\)](#) using a trial-and-error approach and was set equal to $4 \times 10^{-14} \text{ m}^2/\text{s}$. As described extensively in [Guyot et al. \(2014\)](#), the basis of the influence of curvature on the neotissue growth comes from the observation that neotissue grows faster where the curvature is higher and that it does not grow if the curvature is negative or equal to zero ([Bidan et al. 2013](#)). The mean curvature influence function $g(\kappa)$ can therefore be expressed mathematically as follows:

$$g(k) = \begin{cases} -\kappa & \text{if } \kappa > 0 \\ 0 & \text{if } \kappa \leq 0 \end{cases}, \quad (14)$$

where κ is the local mean curvature ($\kappa = \nabla \cdot \mathbf{n}_\Gamma$) and the second row of Eq. (14) depicts that there is no growth when the curvature is null or negative. The negative sign in Eq. (14) comes from the fact that according to our definition of φ , the normal \mathbf{n}_Γ points toward neotissue, so growth has to be toward the opposite of $\nabla \varphi$. The surface shear stress influence function $f(SS_{\text{surf}})$ (unit less) was inspired by [Nava et al. \(2013\)](#) (Fig. 1d) and defined as a continuous function

$$f(SS_{\text{surf}}) = \begin{cases} 0.5 + \frac{0.5 \cdot SS_{\text{surf}}}{a_1} & 0 \leq SS_{\text{surf}} < a_1 \\ 1 & a_1 \leq SS_{\text{surf}} < a_2 \\ \frac{SS_{\text{surf}} - a_3}{a_2 - a_3} & a_2 \leq SS_{\text{surf}} < a_3 \\ 0 & a_3 \leq SS_{\text{surf}} \end{cases}$$

This function was established in order to have an optimal shear stress influence that enhances the growth ($a_1 < SS_{\text{surf}} < a_2$) and a critical threshold ($SS_{\text{surf}} > a_3$) above which shear stress inhibits the cells and growth cannot occur

Table 1 Model parameters used for the calculation of the neotissue growth rate v_G

Parameter	Value	References
Neotissue porosity, ψ	90 %	Guyot et al. (2015)
Neotissue micropore size, δ	50 μm	Guyot et al. (2015)
Neotissue growth rate, A	$4 \times 10^{-14} \text{ m}^2/\text{s}$	Determined from Papantoniou et al. (2014)
Minimal shear stress value enhancing neotissue growth, a_1	0.01	Chapman et al. (2014)
Maximal shear stress value enhancing neotissue growth, a_2	0.03	Chapman et al. (2014)
Critical shear stress value, a_3	0.05	Chapman et al. (2014)

anymore; in this study, a_1 , a_2 and a_3 were, respectively, set to 0.01, 0.03 and 0.05 Pa ([Chapman et al. 2014](#)). Table 1 summarizes all the parameters used in the calculation of the neotissue growth velocity v_G .

2.4 Implementation

The full model was implemented with the free partial differential equation solver *FreeFem++* ([2012](#)). The computational domain (see Fig. 1a) chosen consisted of the part of the perfusion bioreactor chamber comprising the entire scaffold including 2 mm of the chamber at each scaffold side. This was done in order to avoid numerical refluxes and was meshed with approximately 3 million tetrahedrons. The numerical problem was solved in parallel using a 12 core facility. In order to avoid unnecessary computational effort, the Brinkman equation was solved on only one quarter of the full mesh cut along the flow axis and with respect to symmetrical boundary condition.

2.5 Summary of experimental setup

In this study, results presented in [Papantoniou et al. \(2014\)](#) were used in a first calibration and validation setup. The setup of the experiment is briefly repeated below. Three-dimensional additive manufactured open porous Ti6Al4V scaffolds ($\emptyset = 6 \text{ mm}$, $h = 6 \text{ mm}$, porosity = $73 \pm 1 \%$, strut diameter = $245 \pm 2 \text{ mm}$ and pore size = $755 \pm 3 \text{ mm}$), produced on an in-house developed selective laser melting machine ([Van Bael et al. 2011](#)) were used. Human periosteal-derived stem cells (hPDCs, one of the known sources of MSCs) were isolated from periosteal biopsies of different donors as described previously ([Eyckmans et al. 2006](#)) and expanded in culture flasks. When a sufficient amount of these

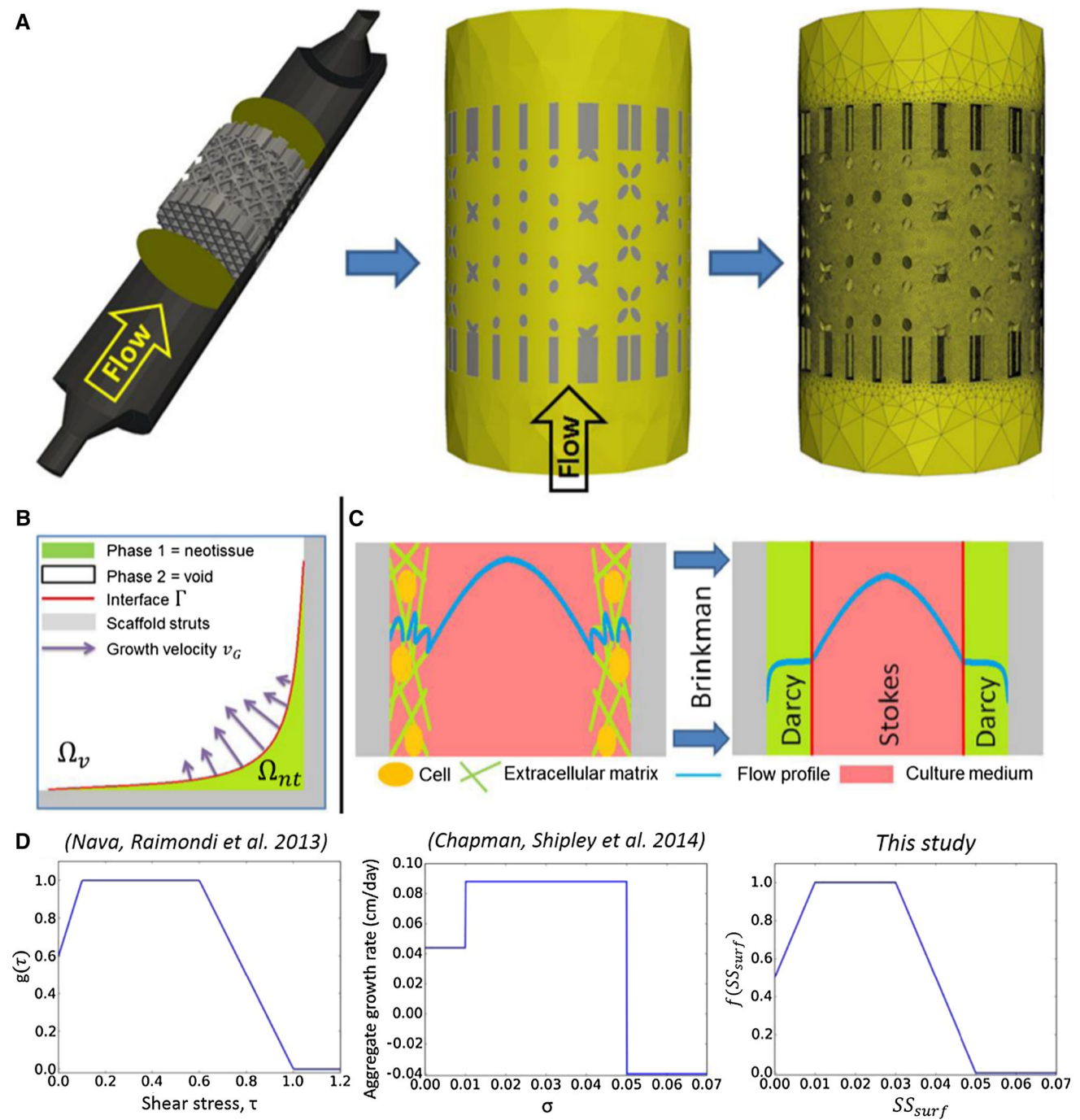


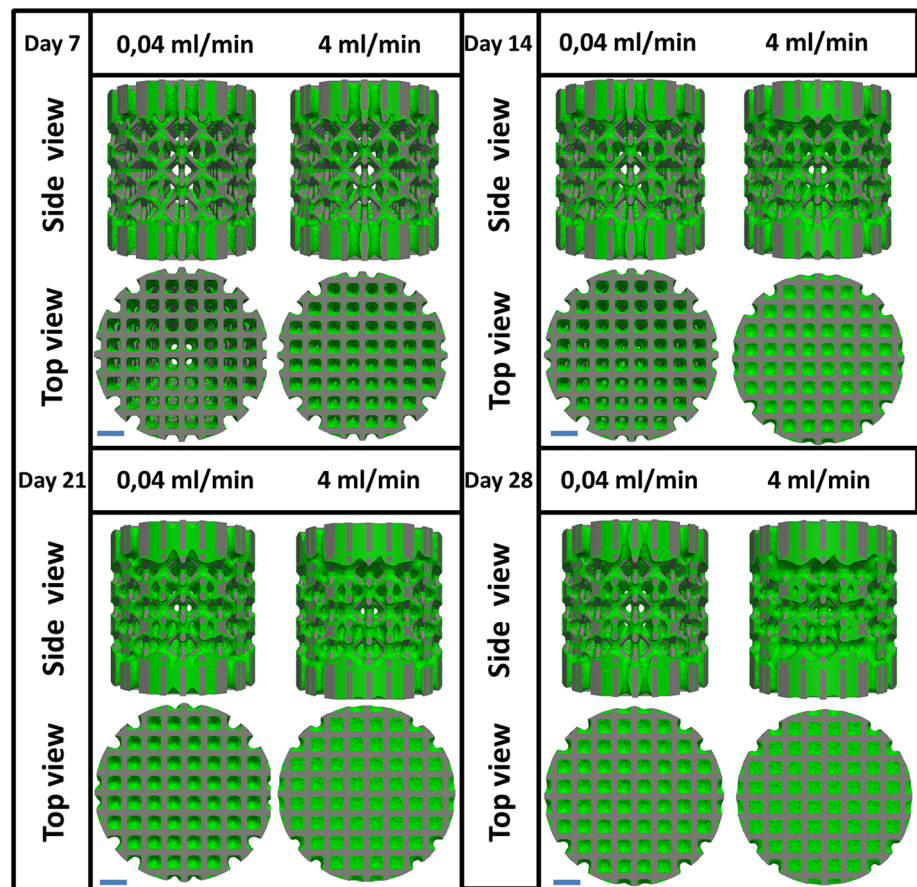
Fig. 1 Model setup. **a** Representation of the scaffold and the bioreactor chamber; the region of interest is delimited by two yellow circles. The scaffold is then removed from a cylinder representing the delimited area. Finally, a mesh is created in the computational domain. **b** Schematic representation of curvature-driven neotissue growth using the level

set method. **c** Schematic representation of the Brinkman approximation used in this study. **d** The influence of shear stress on the neotissue growth velocity in this study (right) is a combination of the continuous shape proposed by Nava et al. (2013) and the values by Chapman et al. (2014) (middle)

cells was produced in this 2D culture (number of population doublings = 15), cells were harvested by trypsinization with Tryple Express (Invitrogen) and seeded on the scaffolds, which marked the start of the bioreactor experiment. The TE constructs were cultured in an in-house developed bioreac-

tor for 14, 21 and 28 days under dynamic culture conditions ($n = 9$ per flow rate—in triplicate per time point). Two different perfusion flow rates were used: 4 ml/min (Q_1 , high) and 0.04 ml/min (Q_2 , low). After culture, three constructs for each time point were prepared for contrast-enhanced nanofo-

Fig. 2 Neotissue growth (green) on scaffold (gray) at different time points for two different flow rates and two different views (direction of flow rate is from bottom to top in side view). Gradual scaffold pore closure can be observed. Scale bar represents 1 mm



cus Computed Tomography (NanoCT) imaging (Kerckhofs et al. 2013) allowing for visualization and quantification of the neotissue volume formed inside the constructs.

3 Results

The model was run for different flow rates according to the experimental setup described in Papantoniou et al. (2014). Simulations show a significant difference between the two conditions regarding the total amount of neotissue that has been produced at different time points (Figs. 2, 3). Indeed, under the high flow rate, the local shear stress acting on the neotissue interface is higher than for the lowest flow rate, resulting in an acceleration of neotissue growth. Although differences can be observed between the simulations and experiments, the simulations are capable of capturing the experimentally observed differences between the two flow rates in terms of volume filling (Fig. 3b). The model was also able to compute quantitative data (shown in Fig. 4) regarding important culture variables during neotissue growth such as pressure drop across the scaffold along the flow axis, average surface and inner shear stresses, giving an overview of different mechanical stimuli acting on cells over culture time.

The pressure drop (Fig. 4a) across the scaffold varied from almost 4 Pa in the first days of culture to 11 Pa at day 28 for the high flow rate Q_1 , while it ranged from 0.03 to 0.08 Pa for the low flow rate Q_2 in an equivalent period of time. The surface shear stresses (Fig. 4b) and inside shear stresses (Fig. 4c) differed by a factor of 100 between the two different flow rates. For both flow rates, the inner shear stress, the stress acting on cells embedded into the neotissue, can be around 3 (for early time points) to 20 (for late time points) times bigger than the interface shear stress acting on cells at interface in contact with the free flow. Figure 5 shows how the flow regime changes from when the scaffold is almost empty (Fig. 5a) to where it is partially filled (Fig. 5b). Figure 6 depicts the local growth velocity v_G showing the influence of the distributed shear stress as well as the local mean curvature of the surface. Maximal neotissue growth velocities of 3 and 7 $\mu\text{m}/\text{day}$ were obtained for the low and high flow rates, respectively.

4 Discussion

Understanding spatiotemporal cell growth in dynamic cultures constitutes a challenge in TE, in particular the quantification, distribution and interplay between scaffold geom-

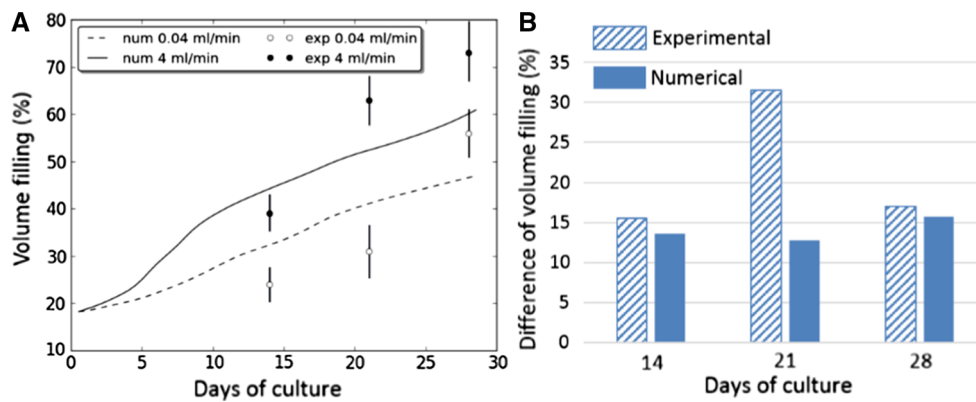


Fig. 3 Comparison between simulations and experimental results (Papantoniou et al. 2014). **a** Evolution of volume filling over culture time for the two different flow rates used in this study. Experimental results are presented through the mean and standard deviation ($n = 3$).

b Quantitative differences in volume filling between the different flow rates, indicating that the simulated differences are similar to those experimentally observed

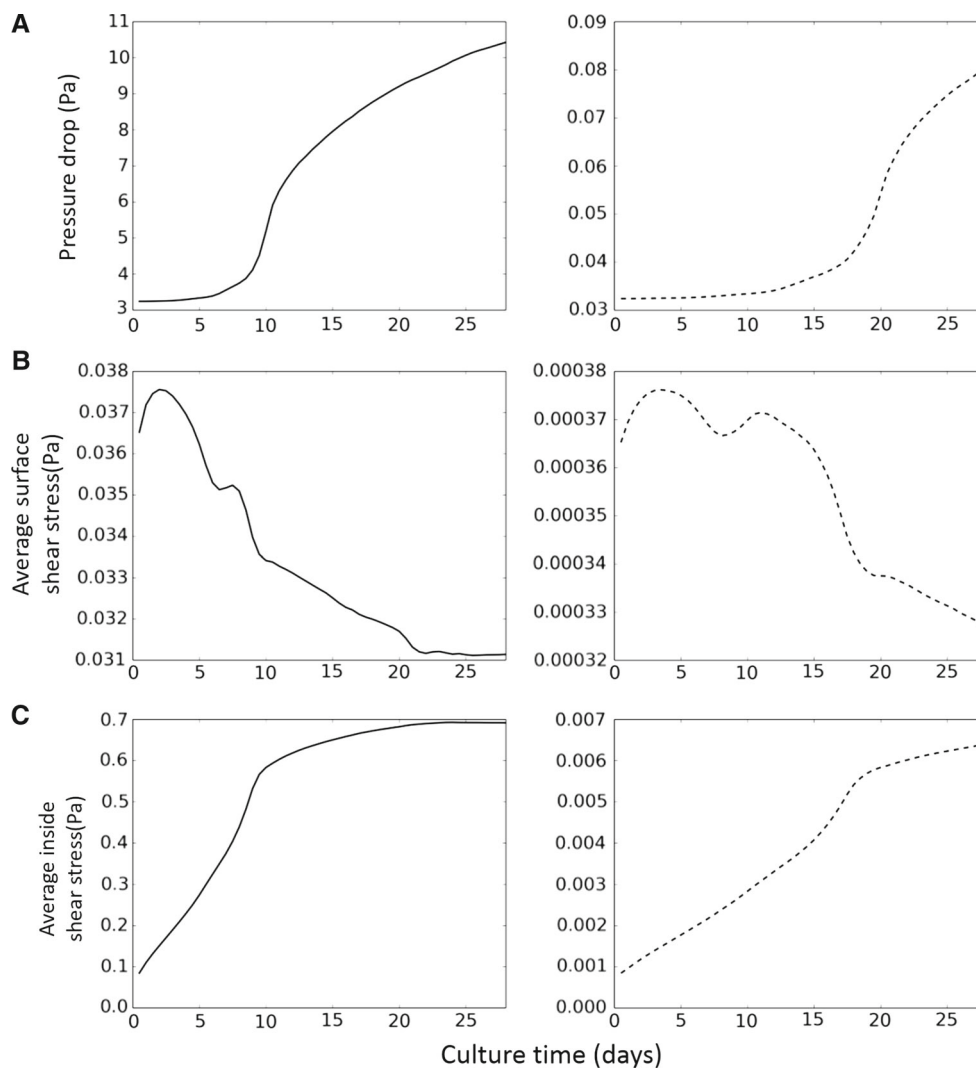


Fig. 4 Mechanical characterization of the predicted tissue growth for flow rates Q_1 (4 ml/min, left) and Q_2 (0.04 ml/min, right). **a** Pressure drop between the entrance and the exit of the scaffold. **b** Average neotis-

sue surface shear stress. **c** Average inside neotissue shear stress. Notice the difference in scale on the vertical axes between left and right figures

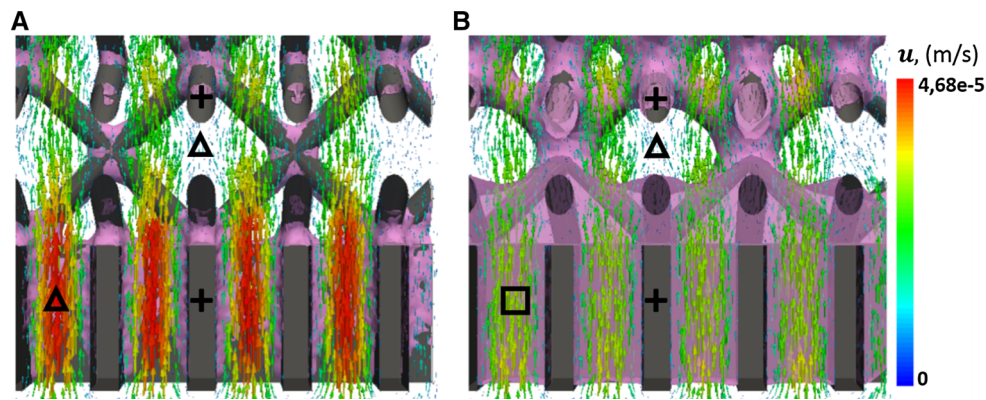
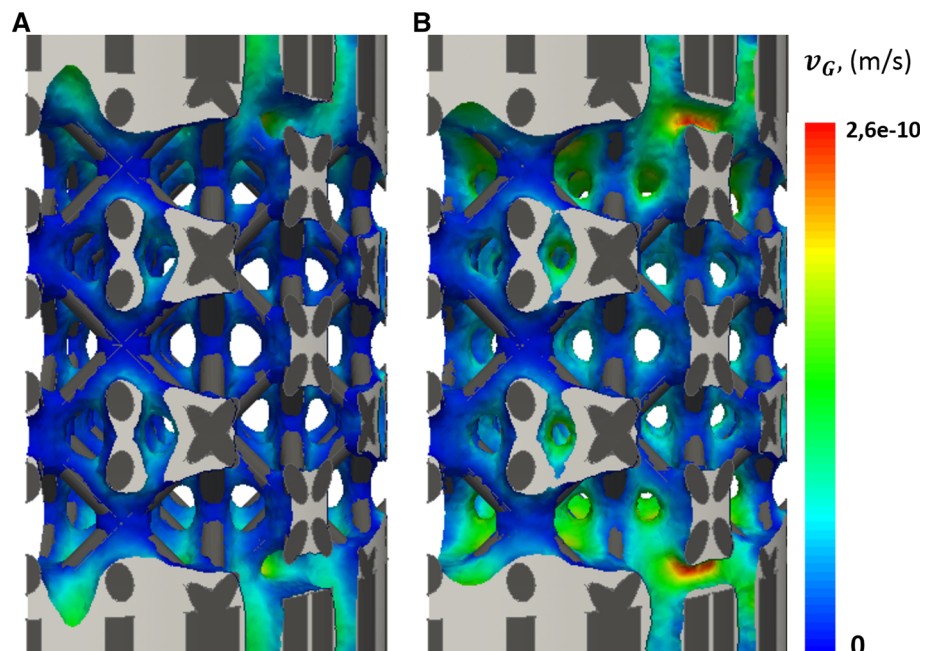


Fig. 5 Close-up view on a section of the scaffold illustrating the different flow profiles (\mathbf{u}) at early (**a**) and late (**b**) time points (neotissue volume is indicated in pink). **a** The scaffold is almost empty, so the flow is mostly ruled by the Stokes equation leading to Poiseuille flow in the

bottom part. **b** The *bottom part* of the scaffold is completely filled with neotissue, so the flow profile in this area is ruled by the Darcy equation. *Plus* scaffold, *square* neotissue, *triangle* void

Fig. 6 Local distribution of the neotissue growth velocity v_g (m/s) at the neotissue–void interface at 28 days for flow rates Q_2 (0.04 ml/min, *left*) and Q_1 (4 ml/min, *right*). The neotissue is indicated in *light gray*



etry, shear stress and neotissue growth. The present model provides a foundation that will allow the quantitative investigation of the effect of shear stresses on cell growth and ECM production, which today is still not well understood. The most important contribution of this study is the extension of a previously developed model of local curvature-dependent neotissue growth to incorporate the influence of the local shear stresses on the neotissue growth, on complete scaffolds in 3D. The importance of 3D models in comparison with 2D has been shown by Nava et al. (2013), the latter suffering from a lack of accurate representation which leads to loss of information and an incorrect parameter estimation.

Recent experimental observations have revealed that hPDCs (the MSC source used in this study) may grow in

the third dimension by bridging scaffold struts, leading to complete filling of scaffold pores when cultured in perfusion bioreactors in glucose-based growth medium (Sonnaert et al. 2014) and in growth factor containing osteogenic medium (Papantoniou et al. 2013). NanoCT imaging has been employed to confirm that complete pore closure could be obtained depending on bioreactor operating conditions (Papantoniou et al. 2014). Similar 3D cell growth behavior upon seeding on scaffolds has been also observed for other cell types such as human bone marrow MSCs (Zhao et al. 2005; Li et al. 2009), primary fibroblasts (Joly et al. 2013) and cell lines such as MC3T3-E1 pre-osteoblast cells (Komareddy et al. 2010). This opens the possibility to create 3D in vitro tissue-like structures where cells may grow indepen-

dently of the initial scaffold surface allowing for the study of the interaction between cells and their own ECM and the culture environment. Additionally, this means that when simulating the experimentally observed void filling due to 3D neotissue growth, models should take into account the specificity of the experimentally used cell type (Chapman et al. 2014). In this work, we attempt to investigate this for adult stem cell types in particular for hPDCs.

Neotissue growth kinetics in 3D dynamic and scaffold-based culture setups has been linked with oxygen level (Zhao et al. 2005), shear stress (Nava et al. 2013) and scaffold geometry—in particular curvature (Bidan et al. 2013; Knychala et al. 2013). In our study, oxygen was not investigated since for the flow rate and scaffold dimensions used in this work, taking into account the oxygen consumption rate of hPDCs (Lambrechts et al. 2014), there is no significant oxygen drop detected from inlet to outlet. Therefore, the assumption that the whole cell population is exposed to the same level of dissolved oxygen tension (atmospheric) seems to be justified. When other flow regimes and/or other cell types will be studied, this assumption has to be re-evaluated. An additional assumption was the existence of an initial single cell layer at the start of the simulations. This layer was assumed to be 20 μm based on 2D suspended MSC diameter values (Darling et al. 2008), leading to an initial filling percentage of 18 %. Provided that a high number of cells are used for cell seeding (Chen et al. 2011), a homogeneous distribution can indeed be achieved across the scaffold. This step has been studied in detail for regular geometry scaffolds (Melchels et al. 2011). The initial filling percentage is likely an overestimation of the real filling and is (in its current way of calculating) dependent on the available surface of the scaffold under study. With the currently used measurement technique (NanoCT), the experimental value for the initial filling cannot be obtained due to the absence of matrix produced by the cells immediately after seeding. This parameter therefore merits further study in future work. Neotissue shrinkage/loss due to cell death was not incorporated in the presented model; however, there is a possibility that this shrinkage/loss occurs for those cases where excessively harsh culture conditions are developed, i.e., very low dissolved oxygen tension (anoxia) and glucose concentration or high lactate concentration (Flaibani et al. 2010). Further efforts are required in order to incorporate the aforementioned physicochemical components in our model. However, this is out of the scope of the present study, where geometry and fluid dynamics are the main regulators of neotissue growth.

In this study, neotissue growth velocity was coupled to the local scaffold topography (curvature) (Guyot et al. 2014) and local fluid flow-induced shear stress. Shear stress was modeled to enhance increasingly neotissue growth from 0 to a_1 reaching a maximum value between a_1 and a_2 (equal to 0.01 and 0.03 Pa, respectively). The lower amount of neotissue

observed at the periphery of the scaffolds is due to the low values of fluid flow-induced shear stresses at that location. This in turn is due to the flow demonstrating a Poiseuille profile when entering the scaffold, thereby positively influencing to a greater extent the neotissue formation at the center of the scaffold. When the shear stress reaches threshold a_3 equal to 0.05 Pa, its effect on neotissue growth was modeled to change into a prohibitive one with decreasing neotissue growth for increasing shear stresses beyond a_3 . Experimental observations of 0.015 Pa as an optimum shear stress level for human bone marrow MSCs cultured in perfusion bioreactors confirmed this hypothesis (Li et al. 2009). A similar range of shear stresses has been reported for human bone marrow MSCs by Grayson et al. (2010) although these values referred to empty scaffold geometries. We have recently experimentally observed the adverse effects of excessive shear stress on neotissue growth by hPDCs in perfusion bioreactors resulting in inhomogeneous tissue-engineered constructs (Papantoniou et al. 2014). This was observed for shear stress values in excess of 0.05 Pa which is the threshold value used in this study. Interestingly (McCoy et al. 2012) estimated a critical threshold for human bone MSC detachment from irregular scaffolds at 0.088 Pa closely matching the one used here, taking into account the differences in scaffold architecture and cell type.

The growth velocity term A was estimated in a trial-and-error fashion based on in-house experimental observations (Papantoniou et al. 2014) measuring neotissue growth on the simulated scaffold for the low flow rate Q_2 . The prediction obtained for the high flow rate Q_1 shows an increase in volume filling, similar to the experimental data (Fig. 3b). The discrepancy observed between experimental and computationally derived neotissue growth kinetics seen in Fig. 3 could be attributed to numerical and physical factors. For the former (numerical factor), we did not go through an objective and rigorous optimization process to find the value for A because of the insufficient quantity of experimental data available. In a follow-up study, dedicated experimental data will be generated to parametrize the model. As to the latter (physical factor), neotissue growth kinetics do not solely depend upon scaffold geometry and shear stress magnitude. The introduction in the model of additional physicochemical parameters that are well known for their influence on neotissue growth such as dissolved oxygen tension (Grayson et al. 2007; Santos et al. 2010), glucose concentration (Saki et al. 2013) and lactate concentrations (Schop et al. 2009) in the medium could help to improve the agreement between experimentally and computationally determined values. Even though for the experiments used in this study (Papantoniou et al. 2014) no global changes in oxygen tension were observed between the inlet and outlet for the flow rate and cell source used, the model allows to quantify these variable throughout the entire scaffold, potentially showing pockets of decreased oxygen

tension (and neotissue growth) coming from improper perfusion due to local geometrical particularities. Additionally, the possibility that higher flow rates might lead to the secretion of more ECM could also explain to a certain extent the differences in volume filling patterns between simulations and experiments.

In a very interesting recent study, neotissue was modeled in 3D by Nava et al. (2013) using the arbitrary Lagrangian–Eulerian (ALE) method to implement mesh movement. However, the flow was only modeled in the void space, which is acceptable for the early growth phase, but is not suitable to simulate complete filling of the scaffold. In this study, we employed the level set method to represent neotissue growth as described previously in Guyot et al. (2014, 2015). This method, separating the movement of the interface from the definition of the mesh, allows tracking the neotissue kinetics until full scaffold pore filling is reached. A maximal neotissue growth velocity of 3 and 7 $\mu\text{m}/\text{day}$ was obtained for the low and high flow rates, respectively, as seen in Fig. 6. The average growth velocities from the present study are the same order of magnitude than the ones estimated in Nava et al. (2013) which were in the order of 1 $\mu\text{m}/\text{day}$ and higher than the values adopted in previous tissue growth models (Sacco et al. 2011). This could be due to the fact that chondrocytes modeled in that work are slow proliferating cells compared to hPDCs.

Numerical predictions obtained in this study (Figs. 4, 5) are in general agreement with published literature with regard to the range of shear stresses calculated at the neotissue interphase during neotissue growth (Boschetti et al. 2006; Cioffi et al. 2006; Lesman et al. 2010; Nava et al. 2013). However, shear stresses developed within the neotissue (SS_{in}) were seen to be an order of magnitude higher than the surface shear stresses. It is interesting to note that the average values obtained for inner shear stress for the high flow rate in this work, reaching 0.7 Pa, compared closely to the ones determined for native bone (1–3 Pa) (Zeng et al. 1994), closer than what has been reported to date for tissue-engineered constructs. In this study, it was assumed that the pores within the neotissue had a size of 50 μm , and this was justified, for our case study, for large hPDC cells whose size has been shown to range between 100–150 μm when fully spread (Eyckmans et al. 2012). This value could become smaller upon 3D confluency when cells ECM secretion might lead to fuller neotissue structures. Interestingly, the calculated inner neotissue (microporous) shear stress magnitude for the selected neotissue pore size matched closely to those determined via single cell simulations (Jungreuthmayer et al. 2009; Verbruggen et al. 2014; Zhao et al. 2014). Empty scaffold simulations may be useful for early time points and have been successfully used to determine stem cell lineage commitment (Song et al. 2013); however, for later culture time points, these models seem to be insufficient.

Using the whole scaffold geometry, it was also possible to determine changing pressure drop values during neotissue growth and subsequent scaffold pore closure. The maximum pressure drop values obtained for the high flow rate, for completely full scaffolds, equaled to 11 Pa for the parameters of this study (cylindrical scaffold dimensions $d = 6 \text{ mm}$, $h = 6 \text{ mm}$; neotissue porosity 90 %, pore size = 50 μm). This value is close to pressure drop measured computationally in microporous polyester scaffolds in flow-through perfusion bioreactors [$\Delta P = 46 \text{ Pa}$, scaffold $h = 20 \text{ mm}$, $d = 100 \text{ mm}$, flow rate 10 ml/min (Podichetty et al. 2014)] but also with experimentally measured pressure drop values for chitosan–gelatin scaffolds [with 80–92 % porosity and pore size $\sim 100 \mu\text{m}$, $d = 100 \text{ mm}$, $h = 2 \text{ mm}$ (Podichetty et al. 2012)]. Pressure drop is a parameter that can be measured online during bioreactor culture and, when linked to this whole scaffold model, could provide a noninvasive readout to monitor neotissue growth in perfusion bioreactors. The continuous secretion of ECM, in particular upon reaching 3D ‘confluency’, is expected to lead a decrease in neotissue permeability. This will occur mostly toward the later stages of perfusion culture. To achieve this in the present model, a time-dependent parameter could be coupled to the porosity parameter making it decrease over time, reflecting ECM deposition. This could be experimentally validated by measuring pressure drop across the tissue-engineered construct over time, for fixed flow rates.

Scaffold design in perfusion bioreactors can affect neotissue growth in two ways. First, due to their geometry, the scaffolds provide topographies that will enhance 3D cell growth and neotissue formation (Melchels et al. 2010; Van Bael et al. 2012). Second, their design will define fluid flow patterns throughout the entirety of the scaffold affecting the mechanical stimuli exerted on the cells (Hutmacher et al. 2008) and the resulting growth kinetics. The computational tool developed in this study could be used to assess biomechanical regimes that will develop in a particular scaffold during neotissue growth but also to evaluate the effect of specific geometries using scaffold CAD designs on these regimes. This model could also suggest ‘ideal’ geometries where shear stress variation exerted on cells across the scaffold could be minimized, resulting thus in a more homogeneous cell population phenotype. The spatiotemporal mapping of shear stress levels will allow to more accurately link phenotypic responses in bioreactors (Yu et al. 2013; Grayson et al. 2011) with the experienced biomechanical microenvironment. Moreover, already observed phenomena such as shear stress-dependent ECM secretion and mineralization (Sikavitsas et al. 2005; Papantoniou et al. 2013) could be also linked to the experienced microenvironment. For their validation, such models will require 3D tools of high resolution such as NanoCT as presented here or synchrotron X ray micro-CT as reported elsewhere (Voronov et al. 2013).

5 Conclusion

In this study, a 3D model of microporous neotissue growth in a dynamic culture environment was presented in which the neotissue growth velocity depends on scaffold geometry and fluid flow-induced shear stress. The obtained simulation results showed a correspondence with established experimental observations. Although the model can be extended to include additional determinants of the growth process, in its current state it is already able to act as a scaffold shape and bioprocess optimization tool, allowing for a control of the flow-induced mechanical stimulation and growth of the neotissue.

Acknowledgments Y.G. is funded by Belgian National Fund for Scientific Research (FNRS) Grant FRFC 2.4564.12. I.P. is funded by an advanced European Research Council grant under the European Union's Seventh Framework Program (FP/2007–2013)/ERC Grant Agreement No. 294191). The research leading to these results has received funding from the European Research Council under the European Union's Seventh Framework Program (FP/2007–2013)/ERC Grant Agreement No. 279100. This work is part of Prometheus, the Leuven R&D division of Skeletal Tissue Engineering.

References

- Bidan CM, Kommareddy KP et al (2012) How linear tension converts to curvature: geometric control of bone tissue growth. *PLoS One* 7(5):e36336
- Bidan CM, Kommareddy KP et al (2013) Geometry as a factor for tissue growth: towards shape optimization of tissue engineering scaffolds. *Adv Healthc Mater* 2(1):186–194
- Boschetti F, Raimondi MT et al (2006) Prediction of the micro-fluid dynamic environment imposed to three-dimensional engineered cell systems in bioreactors. *J Biomech* 39(3):418–425
- Chapman LA, Shipley RJ et al (2014) Optimising cell aggregate expansion in a perfused hollow fibre bioreactor via mathematical modelling. *PLoS One* 9(8):e105813
- Chen Y, Bloemen V et al (2011) Characterization and optimization of cell seeding in scaffolds by factorial design: quality by design approach for skeletal tissue engineering. *Tissue Eng Part C Methods* 17(12):1211–1221
- Cioffi M, Boschetti F et al (2006) Modeling evaluation of the fluid-dynamic microenvironment in tissue-engineered constructs: a micro-CT based model. *Biotechnol Bioeng* 93(3):500–510
- Darling EM, Guilak F (2008) A neural network model for cell classification based on single-cell biomechanical properties. *Tissue Eng Part A* 14(9):1507–1515
- Delaine-Smith RM, Reilly GC (2011) The effects of mechanical loading on mesenchymal stem cell differentiation and matrix production. *Vitam Horm* 87:417–480
- Dos Santos F, Andrade PZ et al (2010) Ex vivo expansion of human mesenchymal stem cells: a more effective cell proliferation kinetics and metabolism under hypoxia. *J Cell Physiol* 223(1):27–35
- Eyckmans J, Lin GL et al (2012) Adhesive and mechanical regulation of mesenchymal stem cell differentiation in human bone marrow and periosteum-derived progenitor cells. *Biol Open* 1(11):1058–1068
- Eyckmans J, Luyten FP (2006) Species specificity of ectopic bone formation using periosteum-derived mesenchymal progenitor cells. *Tissue Eng* 12(8):2203–2213
- Flaibani M, Magrofuoco E et al (2010) Computational modeling of cell growth heterogeneity in a perfused 3D scaffold. *Ind Eng Chem Res* 49(2):859–869
- Gamsjäger E, Bidan C, Fischer F, Fratzl P, Dunlop J (2013) Modelling the role of surface stress on the kinetics of tissue growth in coned geometries. *Acta Biomater* 9(3):5531–5543
- Grayson WL, Bhumiratana S et al (2010) Spatial regulation of human mesenchymal stem cell differentiation in engineered osteochondral constructs: effects of pre-differentiation, soluble factors and medium perfusion. *Osteoarthritis Cartilage* 18(5):714–723
- Grayson WL, Marolt D et al (2011) Optimizing the medium perfusion rate in bone tissue engineering bioreactors. *Biotechnol Bioeng* 108(5):1159–1170
- Grayson WL, Zhao F et al (2007) Hypoxia enhances proliferation and tissue formation of human mesenchymal stem cells. *Biochem Biophys Res Commun* 358(3):948–953
- Guyot Y, Papantoniou I et al (2014) A computational model for cell/ECM growth on 3D surfaces using the level set method: a bone tissue engineering case study. *Biomech Model Mechanobiol* 13:1361–1371
- Guyot Y, Papantoniou I et al (2015) A three-dimensional computational fluid dynamics model of shear stress distribution during neotissue growth in a perfusion bioreactor. *Biotechnol Bioeng*. doi:10.1002/bit.25672
- Hecht F (2012) New development in freefem++. *J Numer Math* 20(3–4):251–265
- Hossain MS, Bergstrom DJ et al (2014) Prediction of cell growth rate over scaffold strands inside a perfusion bioreactor. *Biomech Model Mechanobiol* 14:333–344
- Hossain MS, Chen XB et al (2012) Investigation of the in vitro culture process for skeletal-tissue-engineered constructs using computational fluid dynamics and experimental methods. *J Biomech Eng* 134(12):121003
- Hutmacher DW, Singh H (2008) Computational fluid dynamics for improved bioreactor design and 3D culture. *Trends Biotechnol* 26(4):166–172
- Joly P, Duda GN et al (2013) Geometry-driven cell organization determines tissue growths in scaffold pores: consequences for fibronectin organization. *PLoS One* 8(9):e73545
- Jungreuthmayer C, Donahue SW et al (2009) A comparative study of shear stresses in collagen–glycosaminoglycan and calcium phosphate scaffolds in bone tissue-engineering bioreactors. *Tissue Eng Part A* 15(5):1141–1149
- Kerckhofs G, Sains J, Wevers M, Van de Putte T, Schrooten J (2013) Contrast-enhanced nanofocus computed tomography images the cartilage subtissue architecture in three dimensions. *Eur Cells Mater* 25: 179–189
- Knychala J, Bouropoulos N et al (2013) Pore geometry regulates early stage human bone marrow cell tissue formation and organisation. *Ann Biomed Eng* 41(5):917–930
- Kommareddy KP, Lange C et al (2010) Two stages in three-dimensional in vitro growth of tissue generated by osteoblastlike cells. *Biointerphases* 5(2):45–52
- Lambrechts T, Papantoniou I et al (2014) Model-based cell number quantification using online single-oxygen sensor data for tissue engineering perfusion bioreactors. *Biotechnol Bioeng* 111(10):1982–1992
- Lesman A, Blinder Y et al (2010) Modeling of flow-induced shear stress applied on 3D cellular scaffolds: implications for vascular tissue engineering. *Biotechnol Bioeng* 105(3):645–654
- Li DQ, Tang TT et al (2009) Effects of flow shear stress and mass transport on the construction of a large-scale tissue-engineered

- bone in a perfusion bioreactor. *Tissue Eng Part A* 15(10):2773–2783
- Maes F, Ransbeeck P et al (2009) Modeling fluid flow through irregular scaffolds for perfusion bioreactors. *Biotechnol Bioeng* 103(3):621–630
- McCoy RJ, Jungreuthmayer C et al (2012) Influence of flow rate and scaffold pore size on cell behavior during mechanical stimulation in a flow perfusion bioreactor. *Biotechnol Bioeng* 109(6):1583–1594
- McCoy RJ, O'Brien FJ (2010) Influence of shear stress in perfusion bioreactor cultures for the development of three-dimensional bone tissue constructs: a review. *Tissue Eng Part B Rev* 16(6):587–601
- Melchels FP, Barradas AM et al (2010) Effects of the architecture of tissue engineering scaffolds on cell seeding and culturing. *Acta Biomater* 6(11):4208–4217
- Melchels FP, Tonnarelli B et al (2011) The influence of the scaffold design on the distribution of adhering cells after perfusion cell seeding. *Biomaterials* 32(11):2878–2884
- Nabovati ALE, Sousa ACM (2009) A general model for the permeability of fibrous porous media based on fluid flow simulations using the lattice Boltzmann method. *Compos Part A* 40:860–869
- Nava MM, Raimondi MT et al (2013) A multiphysics 3D model of tissue growth under interstitial perfusion in a tissue-engineering bioreactor. *Biomech Model Mechanobiol* 12(6):1169–1179
- Papantoniou I, Guyot Y et al (2014) Spatial optimization in perfusion bioreactors improves bone tissue-engineered construct quality attributes. *Biotechnol Bioeng* 111(12):2560–2570
- Papantoniou I, Sannaert M et al (2014) Three-dimensional characterization of tissue-engineered constructs by contrast-enhanced nanofocus computed tomography. *Tissue Eng Part C Methods* 20(3):177–187
- Papantoniou Ir I, Chai YC et al (2013) Process quality engineering for bioreactor-driven manufacturing of tissue-engineered constructs for bone regeneration. *Tissue Eng Part C Methods* 19(8):596–609
- Patrachari AR, Podichetty JT et al (2012) Application of computational fluid dynamics in tissue engineering. *J Biosci Bioeng* 114(2):123–132
- Pham NH, Voronov RS et al (2012) Predicting the stress distribution within scaffolds with ordered architecture. *Biorheology* 49(4):235–247
- Podichetty JT, Bhaskar PR et al (2014) Modeling pressure drop using generalized scaffold characteristics in an axial-flow bioreactor for soft tissue regeneration. *Ann Biomed Eng* 42(6):1319–1330
- Podichetty JT, Dhane DV et al (2012) Dynamics of diffusivity and pressure drop in flow-through and parallel-flow bioreactors during tissue regeneration. *Biotechnol Prog* 28(4):1045–1054
- Porter B, Zauel R et al (2005) 3-D computational modeling of media flow through scaffolds in a perfusion bioreactor. *J Biomech* 38(3):543–549
- Raimondi MT, Boschetti F et al (2004) The effect of media perfusion on three-dimensional cultures of human chondrocytes: integration of experimental and computational approaches. *Biorheology* 41(3–4):401–410
- Rauh J, Milan F et al (2011) Bioreactor systems for bone tissue engineering. *Tissue Eng Part B Rev* 17(4):263–280
- Rumpler M, Woesz A et al (2008) The effect of geometry on three-dimensional tissue growth. *J R Soc Interface* 5(27):1173–1180
- Sacco R, Causin P et al (2011) A multiphysics/multiscale 2D numerical simulation of scaffold-based cartilage regeneration under interstitial perfusion in a bioreactor. *Biomech Model Mechanobiol* 10(4):577–589
- Saki N, Jalalifar MA et al (2013) Adverse effect of high glucose concentration on stem cell therapy. *Int J Hematol Oncol Stem Cell Res* 7(3):34–40
- Schop D, Janssen FW et al (2009) Growth, metabolism, and growth inhibitors of mesenchymal stem cells. *Tissue Eng Part A* 15(8):1877–1886
- Sethian JA (1999) Level set methods and fast marching methods: evolving interfaces in computational geometry, fluid mechanics, computer vision, and materials science. Cambridge University Press, Cambridge
- Sikavitsas VI, Bancroft GN et al (2005) Flow perfusion enhances the calcified matrix deposition of marrow stromal cells in biodegradable nonwoven fiber mesh scaffolds. *Ann Biomed Eng* 33(1):63–70
- Song MJ, Dean D et al (2013) Mechanical modulation of nascent stem cell lineage commitment in tissue engineering scaffolds. *Biomaterials* 34(23):5766–5775
- Sonnaert M, Papantoniou I et al (2014) Human periosteal-derived cell expansion in a perfusion bioreactor system: proliferation, differentiation and extracellular matrix formation. *J Tissue Eng Regen Med*. doi:10.1002/term.1951
- Truscello S, Schrooten J et al (2011) A computational tool for the upscaling of regular scaffolds during in vitro perfusion culture. *Tissue Eng Part C Methods* 17(6):619–630
- Van Bael S, Chai YC et al (2012) The effect of pore geometry on the in vitro biological behavior of human periosteum-derived cells seeded on selective laser-melted Ti6Al4V bone scaffolds. *Acta Biomater* 8(7):2824–2834
- Van Bael S, Kerckhofs G et al (2011) Micro-CT-based improvement of geometrical and mechanical controllability of selective laser melted Ti6Al4V porous structures. *Mater Sci Eng Struct Mater Prop Microstruct Process* 528(24):7423–7431
- Verbruggen SW, Vaughan TJ et al (2014) Fluid flow in the osteocyte mechanical environment: a fluid–structure interaction approach. *Biomech Model Mechanobiol* 13(1):85–97
- Voronov R, VanGordon S et al (2010) Computational modeling of flow-induced shear stresses within 3D salt-leached porous scaffolds imaged via micro-CT. *J Biomech* 43(7):1279–1286
- Voronov RS, VanGordon SB et al (2013) 3D tissue-engineered construct analysis via conventional high-resolution microcomputed tomography without X-ray contrast. *Tissue Eng Part C Methods* 19(5):327–335
- Wang YK, Chen CS (2013) Cell adhesion and mechanical stimulation in the regulation of mesenchymal stem cell differentiation. *J Cell Mol Med* 17(7):823–832
- Whittaker RJ, Booth R et al (2009) Mathematical modelling of fibre-enhanced perfusion inside a tissue-engineering bioreactor. *J Theor Biol* 256(4):533–546
- Yu X, Botchwey EA, Levine EM, Pollack S.R, Laurencin CT (2004) Bioreactor-based bone tissue engineering: the influence of dynamic flow on osteoblast phenotypic expression and matrix mineralization. *Proc Natl Acad Sci United States of America*, 101(31):11203–11208
- Zeltinger J, Landeen LK, Alexander HG, Kidd ID, Sibanda B (2001) Development and characterization of tissue-engineered aortic valves. *Tissue Eng* 7(1):9–22
- Zeng Y, Cowin SC et al (1994) A fiber-matrix model for fluid-flow and streaming potentials in the canaliculi of an osteon. *Ann Biomed Eng* 22(3):280–292
- Zhao F, Pathi P et al (2005) Effects of oxygen transport on 3-d human mesenchymal stem cell metabolic activity in perfusion and static cultures: experiments and mathematical model. *Biotechnol Prog* 21(4):1269–1280
- Zhao F, Vaughan TJ et al (2014) Multiscale fluid–structure interaction modelling to determine the mechanical stimulation of bone cells in a tissue engineered scaffold. *Biomech Model Mechanobiol* 14:231–243